The 7th Annual IEEE International Conference on
Cyber Technology in Automation, Control and Intelligent Systems
July 31-August 4, 2017, Hawaii, USA

Motion Planning for Ricochetal Brachiation Locomotion of Bio-primitive Robot

Hongtai Cheng, *Member, IEEE,* Chongjie Rui, Lina Hao, *Member, IEEE*

***Abstract*— Brachiation is a special form of locomotion used by primates swinging from branches to branches with their upper limbs. Primates are capable of adapting their behavior according to different situations. Among them, Ricochetal Brachiation is quite a sophisticated one which can fly primates across a very long distance. Ricochetal Brachiation requires precise coordination of two brachiating and one free-flying phases. The tight coupling, nonlinear and underactuated characteristics bring great challenges on motion flexibility and controller robustness. This paper intends to solve those two problems by planning feasible and flexible motion trajectories on-the-fly, which deals with the planning problem in ricochetal brachiation process with different distance, attitude and energy variations. The key of ricochetal motion planning is to determine the free fly trajectory. However, tight coupling of three phases introduces too much uncertainty. To reduce the search space, geometric, translational, rotational and brachiation pattern constraints are explored. The rotational constraints brought by momentum conservation is analyzed to discover the internal bounding conditions and landing patterns. Natural constraint planner(NCP) is proposed to organize the conditions and find feasible ricochetal motion. Simulation results show effectiveness and flexibility of the proposed methodology.**

I. Introduction

Bio-primate robot is the bionic robot which mimics the locomotion of primate animals. The primate animals such as gibbons and siamang are able to "fly" swiftly through the forest canopy by brachiation. Primates are capable of adapting their behavior according to different required speed and handholds spacing situations. Typically, Continuous Contact Brachiation(CCB) and Ricochetal Brachiation(RB) (or called "fast brachiation") are the most commonly used ones. Both brachiation gaits containts a "single contact swing phase", when the body is hung on the handholds by a single arm. The difference is the "double contact phase" for CCB gait versus "flight phase" for RB gait, during which there is no contact to the handholds and the center-of-gravity follows a parabolic trajectory. CCB and RB are similar to walking and running in bipedal locomotion. CCB is slow and with close handholds spacing. RB is for large handholds spacings and can generate very high speed and fly over a very long distance. In some circumstances, the gibbons can fly as far as 10 meters [1].

Various theories are proposed to explain the dynamics of this locomotion. Pendulum like swing model and ballistic flight model are commonly used to describe the brachiation process. Point-mass model [2], distributed-mass model, two link model, three/five link model [3], etc. are typically used to modeling the primates body structure [4]. Also, the force profile and the energy change during the brachiation process, the collision in phase switch process, the assisting movement of the leg, the safe margin and the minor variations in CCB are studied [5], [6].

H. Cheng, C. Rui and L. Hao are with the Department of Mechanical Engineering and Automation, Northeastern University, China, chenght@me.neu.edu.cn

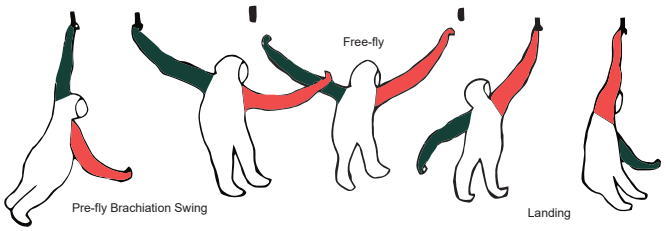

Fig. 1. Diagram illustrates the ricochetal brachiation of a gibbon.

Bio-primate robot with brachiation capability will be useful in many scenarios such as power line inspection [7], forest maneuver [8], disaster rescue, et al. In order to mimic the brachiation locomotion, a variety of Bio-primate robots had been developed. Fukuda's research team contributed many of them. They first developed a two-link Brachiation Mobile Robot [9], then the 7 and 13 degree-of-freedoms Brachiation Mobile Robot(BMR) to improve the dexterity [10], [11]. Kajima et al. [12] designed and manufactured the "Robot I-III Gorilla", and successfully implemented brachiation and bipedal walking motion. Control algorithms such as Empirical learning method [10], try and error learning method, target dynamics control method, virtual constraint based method, et .al were proposed to realize the continuous contact brachiation.

Nishimura proposed a final state control strategy with error learning algorithm to achieve the control of three-link Brachiation robot [13], Meghdari Solves the trajectory planning and control problem with both horizontally and vertically uneven distributed handholds [14].

Ricochetal Brachiation requires precise coordination of two brachiating and one free-flying phases. As stated in [15], this problem is tightly related to flip maneuver of a jumping robot [16], posture control of free flying robots [17], space robots [18] etc. Timm analyzed different bio-primate robot structures and planed feasible trajectory including CCB and RB based on genetic optimization algorithm [19]. Nakanishi studied two-link Brachiation Mobile Robot and developed the control algorithm to complete "leap" motion using simulation [15]. However, as claimed by Nakanishi, due to physical limitations, such locomotion cannot be realized

978-1-5386-0490-8/17/$31.00 © 2017 IEEE

Authorized licensed use limited to: University of Pennsylvania. Downloaded on May 23,2025 at 14:26:01 UTC from IEEE Xplore. Restrictions apply.

in their prototypes.

Ricochetal Brachiation requires precise coordination of two brachiating and one free-flying phases. The tight coupling, nonlinear and underactuated characteristics bring great challenges on motion flexibility and controller robustness. This paper intends to solve those two problems by planning feasible and flexible motion trajectories on-the-fly, which deals with the planning problem in ricochetal brachiation process with different distances, attitudes and energy variations.

II. Problem Formulation and Two-link Bio-primate Robot Modeling

A. Ricochetal Brachiation

As shown in Figure 3, typically ricochetal brachiation process is consisted of three phases: Contact Phase I, Flight Phase and Contact Phase II. According to the flight character and phase functions, they can also be called Takeoff Phase(TP), Free-fly Phase(FP), and Landing Phase(LP).

These three phases are divided by two states: Pre-fly State and Post-fly State. These states are the entry and leaving state for the free-fly phase, as shown in Figure 1. They are the goal state of TP and FP respectively. Once they are reached, switching action will be executed to transfer to the next phase. Moreover, usually the LP is also the TP of next ricochetal brachiation steps. Therefore, a continuous ricochetal brachiation is realized.

It is noted for a bio-primate robot with arms, legs and hands, additional kinematics and dynamics should be considered. Usually the solution is not unique. Therefore, it is necessary to find an optimal solution from the point view of energy and time efficiency.

B. Contact Phase Dynamic Modeling

In TP and LP phases, one of the gripper is connected to the substrate and the robot can be seen as a two degree-of-freedoms(DOF) underactuated mechanical systems. The robot structure is shown in Figure 2.

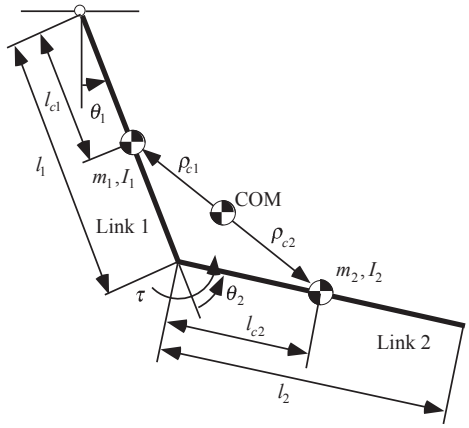

Fig. 2. Diagram of the two-link bio-primate robot.

Where θ_1, θ_2 are the wrist and shoulder joint angles respectively. m_i, I_i, l_i, l_{c_i} are the mass, moment of inertia, length and CoM(Center of Mass) position of link i. ρ_{c_i} is the vector pointing from CoM of the system to CoM of link i. τ is the torque input at the shoulder joint. With these notation, the system's dynamic model can be derived using Lagrange equation:

$$d_{11}\ddot{\theta}_1 + d_{12}\ddot{\theta}_2 + h_1 + \phi_1 = 0 \quad (1)$$

$$d_{21}\ddot{\theta}_1 + d_{22}\ddot{\theta}_2 + h_2 + \phi_2 = \tau \quad (2)$$

where

$$d_{11} = \omega_1 + \omega_2 + 2\omega_3 \cos\theta_2 \qquad \phi_2 = \omega_5 g \sin(\theta_1 + \theta_2)$$
$$d_{22} = \omega_2 \qquad \omega_1 = I_1 + m_1 {l_{c1}}^2 + m_2 {l_1}^2$$
$$d_{12} = d_{21} = \omega_2 + \omega_3 \cos\theta_2 \qquad \omega_2 = I_2 + m_2 {l_{c2}}^2$$
$$h_1 = -\omega_3 \dot{\theta}_2 \sin\theta_2 (2\dot{\theta}_1 + \dot{\theta}_2) \qquad \omega_3 = m_2 l_1 l_{c2}$$
$$\phi_1 = \omega_4 g \sin\theta_1 + \omega_5 g \sin(\theta_1 + \theta_2) \qquad \omega_4 = m_1 l_{c1} + m_2 l_1$$
$$h_2 = \omega_3 {\dot{\theta}_1}^2 \sin\theta_2 \qquad \omega_5 = m_2 l_{c2}$$

Robot physical parameters used in this paper are listed in TABLE I.

TABLE I
Physical Parameters of the Bio-primate Robot

m_1	l_1	l_{c1}	I_1	m_1	l_1	l_{c1}	I_1	g
kg	m	m	kgm^2	kg	m	m	kgm^2	ms^{-2}
1	1	0.5	1/12	1	1	0.5	1/12	9.81

In Equation (1) and (2), there are two DOFs but only one torque input, it is an underactuated mechanical system. Equation (1) is a second order nonholonomic constraints which restraints the dynamics of the mechanical system and brings great challenges in precise motion planning and control.

C. Free-fly Phase Dynamic Modeling

In the FP phase, the robot's gripper releases from the substrate and the whole robot fly along a parabolic trajectory in the air. The FP process is shown in Figure 3.

In Figure 3, a general situation is considered where the adjacent substrates are parameterized by horizontal distance d and vertical height h. l_{c0} and θ_{c0} are the length and angle of robot CoM vector in base frame. β_0 is instantaneous angle between take-off CoM velocity and horizontal axis. R is the horizontal displacement of CoM from takeoff to landing.

During the free-fly process, the only external force is gravity. The translational movement follows a parabolic trajectory. i.e., no matter how the two links move, the CoM trajectory of the robot is determined by (3).

$$\begin{aligned} x_c(t) &= x_{c0} + v_0 \cos\beta_0 t \\ y_c(t) &= y_{c0} + v_0 \sin\beta_0 t - 0.5 g t^2 \end{aligned} \quad (3)$$

Meanwhile, the rotational movement is also determined according to the law of conservation of angular momentum [15].

$$H = c_1[(c_2 + c_3\cos\theta_2)\dot{\theta}_1 + (c_4 + c_5\cos\theta_2)\dot{\theta}_2] = H_0 \quad (4)$$

where

$$\begin{aligned} &c_1 = \tfrac{1}{m_1+m_2}, c_3 = 2m_1m_2(l_1 - l_{c1})l_{c2} \\ &c_2 = m_1(I_1 + I_2) + m_2(I_1 + I_2 + m_1(l_1 - l_{c1})^2 + {l_{c2}}^2) \\ &c_4 = m_1m_2{l_{c2}}^2 + (m_1 + m_2)I_2, c_5 = m_1m_2(l_1 - l_{c1})l_{c2} \end{aligned} \quad (5)$$

Authorized licensed use limited to: University of Pennsylvania. Downloaded on May 23,2025 at 14:26:01 UTC from IEEE Xplore. Restrictions apply.

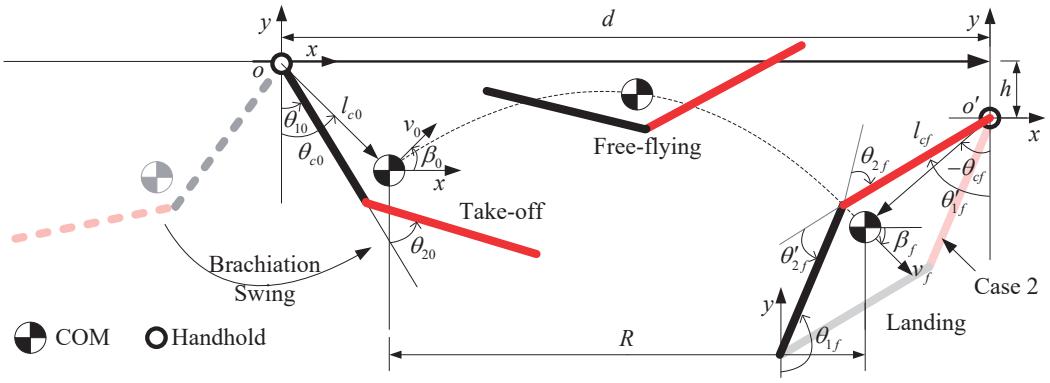

Fig. 3. Ricochetal brachiation process of two-link brachiating robot.

According to (4), there is

$$\dot{\theta}_1 = \frac{H_0}{c_1(c_2 + c_3\cos\theta_2)} - \frac{c_4 + c_5\cos\theta_2}{c_2 + c_3\cos\theta_2}\dot{\theta}_2 \tag{6}$$

Equation (6) indicates that during the free-fly phase, rotation movements of the two links are related. Therefore, although there is only one actuated input in the two-link bio-primate robot system, it is possible to adjust the shape configuration by planning the θ_1, θ_2 together and controlling them through $\dot{\theta}_2$.

Equation (3) and (6) characterize the dynamics during the free-fly phase. However, because H_0, v_0, β_0 and the target states are still not determined, selecting an appropriate solution for ricochetal brachiation requires a joint optimization procedure to plan all the variables.

All the related variables are listed in TABLE II. There are 24 variables which are classified into 3 categories.

TABLE II

UNDETERMINED RICOCHETAL BRACHIATION RELATED VARIABLES

Variables	Count	Description
$l_{c0}, \theta_{c0}, v_0, \beta_0, \theta_{10}, \theta_{20}, \dot{\theta}_{10}, \dot{\theta}_{20}$	8	Pre-fly variables
$l_{cf}, \theta_{cf}, v_f, \beta_f, \theta_{1f}, \theta_{2f}, \dot{\theta}_{1f}, \dot{\theta}_{2f}$	8	Post-fly variables
t_f, R	2	Free-fly variables
Total	18	

Considering the geometric and velocity relations, some of those variables can be calculated with the other and some are irrelevant with the ricochetal planning process, key variables should be determined are $\theta_{c0}, l_{c0}, v, \beta_0, t_f, \theta_{cf}, l_{cf}$. It is noted that all those variables are defined on COM to simplified the planning process.

D. Joint Angle profile during the free-fly process

By analyzing the video of gibbon's ricochetal brachiation locomotion, it is noted that that during the free-fly process, the Arm 2 has a special speed profile: In the begin and end of the fly process, the speed is low; In the middle, the speed is higher. Different from the constant speed assumption given in [15].

This speed profile can be approximated using half sine function. Considering the initial and final value of θ_2, the profile can be derived as

$$\begin{aligned} \dot{\theta}_2(t) &= \frac{\pi}{t_f}\frac{\theta_{2f}-\theta_{20}}{2}\sin\frac{\pi}{t_f}t \\ \theta_2(t) &= -\frac{\theta_{2f}-\theta_{20}}{2}\cos\frac{\pi}{t_f}t + \frac{\theta_{2f}+\theta_{20}}{2} \end{aligned} \tag{7}$$

Although not integrable, this profile generated a very smooth motion of θ_2 during the free-fly process. When $t \to 0$ and $t \to t_f$, $\dot{\theta}_2 \to 0$ and $\theta_2(0) = \theta_{20}, \theta_2(t_f) = \theta_{2f}$.

III. RICOCHETAL BRACHIATION MOTION PLANNING

The goal of ricochetal brachiation motion planning task is to find a feasible solution of the closely interconnected three phases. There are 18 physical variables within the process needed to be determined. Even after simplification, the number is still 7. Furthermore, the solution may not be unique, hence it is quite a difficult procedure to determine a relatively optimal one. To reduce the search space, internal constraint should be further explored.

A. Natural Constraints in Continuous Contact Brachiation

1) Natural Constraints: Continuous contact brachiation is the leading phase in ricochetal brachiation. According to observation of gibbons' motion and Gymnasts' performance, it is noticed that there is a natural constraints of brachiation swing as shown in Figure 4.

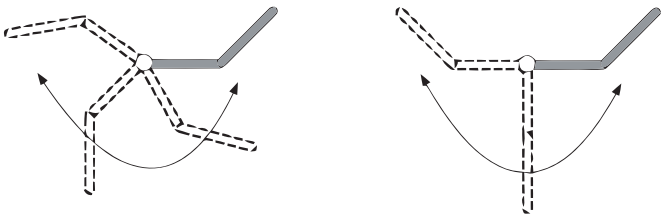

Energy Conservation Constraint Natural Symmetric Constraint

Fig. 4. Natural Constraints within the Bio-primate Robot

In Figure 4, two swing patterns are presented. The left one maintains a fixed shape during swinging while the right one changes the shape according to the swing position. It is easy to verify that the left one maintains a constant energy level like a pendulum while the right one is more natural and maintains a periodic energy oscillation. The right one can be used in energy accumulation process. Quantitative

Authorized licensed use limited to: University of Pennsylvania. Downloaded on May 23,2025 at 14:26:01 UTC from IEEE Xplore. Restrictions apply.

calculation shows that the right one needs less torque and energy consumption. Detailed discussioncan be found in [20].

The right natural symmetric motion pattern can be descried using a linear virtual constraint,

$$\theta_2 = k\theta_1 + b \tag{8}$$

where k, b can be set according to preference. A typical one could be $k = 0.5, b = 0$ which will generate a symmetric motion pattern as shown in Figure 4.

2) Natural Constraints on CoM: The constraints on joint coordinates can be transformed to CoM state variables (l_c, θ_c) as shown in Figure 5(a).

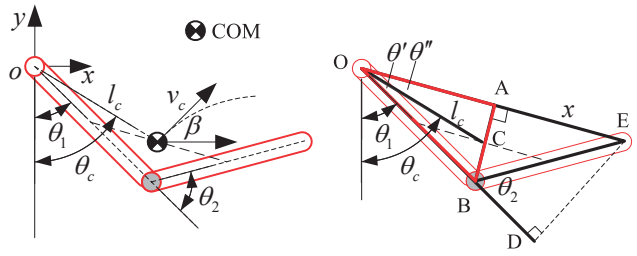

(a) Joint and CoM Variables (b) Geometric Relation

Fig. 5. Natural Constraints on CoM

l_c and θ_c are two important variables in the ricochetal motion planning process. Figure 5(b) shows geometric connection between joint angles and CoM states. Drawing the perpendicular line from E to OB where intersect at D, it is easy to verify that triangular OAB and ODE are similar. One gets:

$$\frac{|\mathrm{AB}|}{|\mathrm{OA}|} = \frac{|\mathrm{DE}|}{|\mathrm{OD}|} \tag{9}$$

Because ODE is a right angle triangle, there is

$$\frac{|\mathrm{DE}|}{|\mathrm{OD}|} = \frac{|\mathrm{BE}|\sin\theta_2}{|\mathrm{OB}| + |\mathrm{BE}|\cos\theta_2} = \frac{\sin\theta_2}{1+\cos\theta_2} \tag{10}$$

Considering triangular OAC, there is

$$\theta'' = \operatorname{atan}\frac{|\mathrm{AC}|}{|\mathrm{OA}|} = \operatorname{atan}\frac{1}{2}\frac{|\mathrm{AB}|}{|\mathrm{OA}|} \tag{11}$$

Therefore, one gets

$$\theta'' = \operatorname{atan}\frac{1}{2}\frac{\sin\theta_2}{1+\cos\theta_2} \tag{12}$$

Furthermore, θ' can be calculated through

$$\theta' = \frac{\theta_2}{2} - \theta'' = \frac{\theta_2}{2} - \operatorname{atan}\frac{1}{2}\frac{\sin\theta_2}{1+\cos\theta_2} \tag{13}$$

$$\theta_c = \theta_1 + \theta' = \theta_1 + \frac{\theta_2}{2} - \operatorname{atan}\frac{1}{2}\frac{\sin\theta_2}{1+\cos\theta_2} \tag{14}$$

Also, it is easy to calculate l_c, i.e. length of OC,

$$l_c = \frac{1}{2}\sqrt{(l_{c1}+l_1)^2 + l_{c2}^2 + 2l_{c2}(l_{c1}+l_1)\cos\theta_2} \tag{15}$$

In summary,

$$\left.\begin{array}{l} l_c = f_l(\theta_2) \\ \theta_c = \theta_1 + f_\theta(\theta_2) \\ \theta_2 = k\theta_1 + b \end{array}\right\} \Rightarrow l_c = f(\theta_c) \tag{16}$$

Therefore, under natural constraints, CoM states variables l_c and θ_c are internally related, which can be used to bound the state variables and reduce the search space.

B. Physical Constraints in Free-fly Phase

The free-fly phase connects both of the pre-fly and post-fly states. It is the key for the ricochetal brachiation motion planning problem. The Free-fly phase is simplified and illustrated in Figure 6.

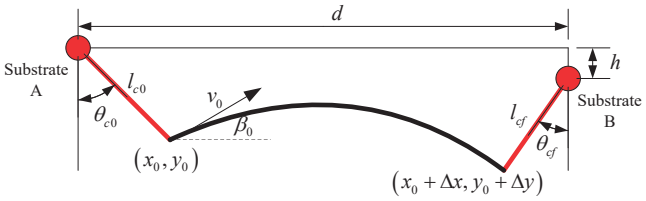

Fig. 6. Free fly process for the Bio-primate Robot

Two adjacent substrates A and B are considered. They have a horizontal distance d and a vertical distance h, where $h < 0$ indicates B is lower than A. The central black curve is CoM flight trajectory(a parabolic trajectory). The left and right red lines are the CoM vector before and after free-fly process.

1) CoM Physical Constraints: Using geometrical and physical theory, one can get the following equations.
The pre-fly CoM coordinates:

$$\begin{aligned} x_0 &= l_{c0}\sin\theta_{c0} \\ y_0 &= l_{c0}\cos\theta_{c0} \end{aligned} \tag{17}$$

The post-fly CoM coordinates:

$$\begin{aligned} x_0 + \Delta x &= d - l_{cf}\sin\theta_{cf} \\ y_0 + \Delta y &= h - l_{cf}\cos\theta_{cf} \end{aligned} \tag{18}$$

The parabolic equation:

$$\begin{aligned} \Delta x &= v_0 t_f \cos\beta_0 \\ \Delta y &= v_0 t_f \sin\beta_0 - 0.5 g t_f^2 \end{aligned} \tag{19}$$

These six equations only describe the CoM's translational motion. The rotation motion is based on joint angles θ_1 and θ_2 and will be discussed in the following subsection.

2) Joint Angle Constraint: As previously mentioned, although the CoM motion is determined, the robot shape can be controlled by adjusting should joint angle $\dot{\theta}_2$. This process is governed by Equation (6). To synchronize the body rotation process with flying and grasping process, a trajectory connecting the initial pre-fly state and final post-fly state should be designed. According to (6), there is

$$\Delta\theta_1(t) = \int_0^t \left(\frac{H_0}{c_1(c_2 + c_3\cos\theta_2)} - \frac{c_4 + c_5\cos\theta_2}{(c_2 + c_3\cos\theta_2)}\dot{\theta}_2\right)\mathrm{dt} \tag{20}$$

Authorized licensed use limited to: University of Pennsylvania. Downloaded on May 23,2025 at 14:26:01 UTC from IEEE Xplore. Restrictions apply.

This is a nonlinear integral equation. As stated in Section II, $\Delta\theta_1$ and $\Delta\theta_2$ are internally related. It is impossible to find universal $\dot{\theta}_2$ profile to synchronize the change of θ_1 and θ_2 if they are not compatible.

In this paper, Equation (7) is chosen as the $\dot{\theta}_2$ profile. The change of θ_2 at $t = t_f$ is

$$\Delta\theta_2\left(t_f\right) = \theta_{2f} - \theta_{20} \tag{21}$$

which naturally meets the requirements. Therefore, the problem is to find proper θ_{10}, θ_{1f} and t_f to match the change of θ_1,

$$\Delta\theta_1\left(t_f\right) = \theta_{1f} - \theta_{10} \tag{22}$$

To reduce the variable involved in the motion planning process, we try to formulate the constraints using CoM variables. Therefore, the joint angle constraint (22) should be converted.

Under the geometric relation shown in Figure 3, θ_{10}, θ_{20} and θ_{c0}, l_{c0} can be calculated using

$$\begin{aligned} \theta_{20} &= \arccos\left(\frac{2l_{c0}^2 - (l_1 + l_{c1})^2 - l_{c2}^2}{2l_{c2}(l_1 + l_{c1})}\right) \\ \theta_{10} &= \theta_{c0} - \tfrac{\theta_{20}}{2} + \arctan\left(\frac{0.5\sin\theta_{20}}{1 + \cos\theta_{20}}\right) \end{aligned} \tag{23}$$

θ_{1f}, θ_{2f} and θ_{cf}, l_{cf} can be calculated using

$$\begin{aligned} \theta_{2f} &= -\arccos\left(\frac{2l_c^2 - (l_1 + l_{c1})^2 - l_{c2}^2}{2l_{c2}(l_1 + l_{c1})}\right) \\ \theta_{1f} &= \pi + \theta_2 - \theta_{cf} - \tfrac{\theta_{20}}{2} + \arctan\left(\frac{0.5\sin\theta_{20}}{1 + \cos\theta_{20}}\right) \end{aligned} \tag{24}$$

To calcuate H_0, $\dot{\theta}_{10}$ and $\dot{\theta}_{20}$ should also be converted using

$$\begin{bmatrix} \dot{\theta}_{10} \\ \dot{\theta}_{20} \end{bmatrix} = R^{-1} \begin{bmatrix} v_0\cos\beta_0 \\ v_0\sin\beta_0 \end{bmatrix} \tag{25}$$

where

$$R = \frac{\begin{bmatrix} m_1 l_{c1} C_1 + m_2\left(l_1 C_1 + l_{c2} C_{12}\right) & m_2 l_{c2} C_{12} \\ m_1 l_{c1} S_1 + m_2\left(l_1 S_1 + l_{c2} S_{12}\right) & m_2 l_{c2} S_{12} \end{bmatrix}}{m_1 + m_2} \tag{26}$$

and C_1, S_1, C_{12}, S_{12} refer to $\cos\theta_{10}, \sin\theta_{10}, \cos(\theta_{10} + \theta_{20}), \sin(\theta_{10} + \theta_{20})$.

With these convension equations, constraint (22) can be converted to

$$e(l_{c0}, \theta_{c0}, l_{cf}, \theta_{cf}, v_0, \beta_0, t_f) = 0 \tag{27}$$

This equation represents the joint angle synchronization in CoM variables form.

C. Multiple Solutions for Free-fly Trajectory Planning

In physical constraints (17), (18), (19) and (27), there are totally 7 equations with 11 variables. The solution is not unique. To find feasible solutions for the free fly process of the ricochetal locomotion, it is necessary to find a reasonable way to reduce the variance.

Currently, there are 4 undetermined variables. 2-3 conditions should be introduced to reduce the search space. Instead of introducing strong symmetrical conditions, the following one is proposed.

1) Natural Constraints Planner(NCP): As previously mentioned in Section III-A, the natural constraints provide additional constraints on the state variables. They can be used to reduce the search space. The auxiliary equations are

$$\begin{aligned} l_{c0} &= f\left(\theta_{c0}\right) \\ l_{cf} &= f\left(\theta_{cf}\right) \end{aligned} \tag{28}$$

To control the flight efficiency and energy level, the flight angle is designated,

$$\beta_0 = \beta_0^d \tag{29}$$

With those three equations, the problem is parameterized with θ_{c0}. Numerical solution can be found by assigning desired parameters. In this paper Nelder-Mead method is used to solve the numerical optimization problem.

IV. Simulation Results

The simulations are based on the physical parameters listed in TABLE I. Three groups of experiments are performed to test effectiveness and adaptiveness of the proposed natural constraits planner and on-the-fly planner.

A. Natural Constraints Planner Example

For a given d, h, Natural Constraints Planner requires the natural constraint parameters (k, b) and takeoff angle β_0 to complete the planning process. In this example, $d = 2.5, h = -0.5, k = 0.5, b = 0, \beta_0 = pi/4$. For the given condition, there is only one feasible solution exists. After optimization, the solution is $\theta_{c0} = 0.7823$, $\theta_{cf} = 0.8393$, $v = 2.7087$ and $t_f = 0.5579$. Snapshots of the ricochetal free-fly plan is plotted in Figure 7. In this figure, besides the robots, the

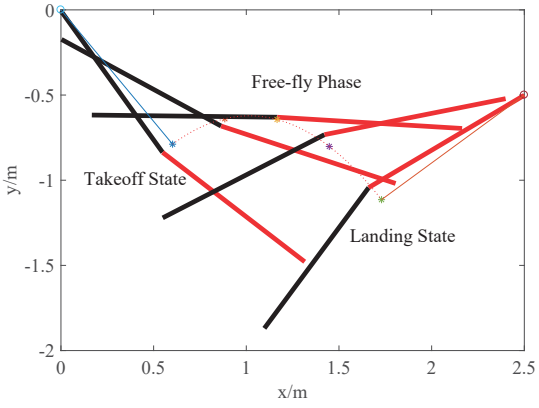

Fig. 7. Snapshots of the ricochetal free-fly process

COM trajectory and vectors are also presented. It can be seen clearly that the robot starts from the initial substrate at (0,0) and finally grabs the substrate at (2.5,-0.5), i.e. a complete ricochetal step. The change of each state variables are given in Figure 8. The COM position (x, y) is fixed no matter how the joint angles changes. x follows a linear function while y follows a quadratic function. θ_2 follows the specifically designed sine function, connecting the initial value and final value smoothly.

Authorized licensed use limited to: University of Pennsylvania. Downloaded on May 23,2025 at 14:26:01 UTC from IEEE Xplore. Restrictions apply.

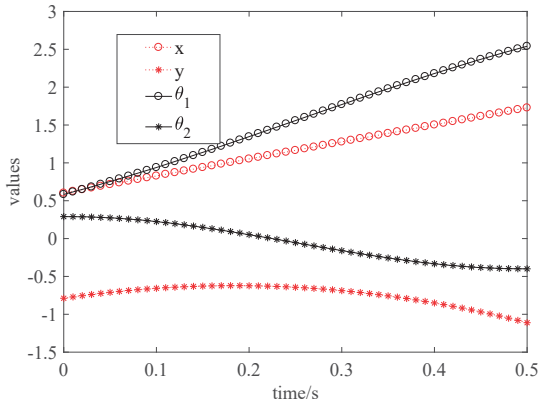

Fig. 8. State variables charts in the ricochetal free-fly process

B. Planning with Different Distances and Heights

In forest, the gibbons have to deal with unstructued environment with randomly distributed substrates. To simulate such feature, ricochetal brachiation with different distances and heights are carried out. d ranges from 3m to 8m while h ranges from -0.5m to 0.5m. β is fixed as $\pi/4$. The planned results are listed in TABLE III.

TABLE III

NCP PLANNED RESULTS WITH DIFFERENT HEIGHTS AND DISTANCES

d	h	β	θ_{c0}	l_{c0}	θ_{cf}	l_{cf}	t_f	v
3	-0.5	$\pi/4$	0.876	0.986	0.728	0.990	0.668	3.351
3	0	$\pi/4$	0.876	0.986	0.738	0.990	0.585	3.813
3	0.5	$\pi/4$	0.876	0.986	0.750	0.990	0.487	4.557
5	-0.5	$\pi/4$	1.007	0.981	0.548	0.994	0.955	5.407
5	0	$\pi/4$	1.007	0.981	0.547	0.994	0.901	5.737
5	0.5	$\pi/4$	1.006	0.981	0.524	0.995	0.846	6.141
8	-0.5	$\pi/4$	1.061	0.979	0.460	0.996	1.246	7.607
8	0	$\pi/4$	1.061	0.979	0.462	0.996	1.204	7.869
8	0.5	$\pi/4$	1.061	0.979	0.461	0.996	1.161	8.161

These experiments show that the proposed method is effective to handle unstructured conditions with different distances and heights.

V. CONCLUSION

This paper proposes a systematic trajectory planning method for ricochetal brachiation of two-link bio-primate robot. The main difficulty for this problem is how to formulating the internal constraints to reduce the search space for feasible solutions. The constraints from four aspects: CoM physical and geometric relation in free-fly phase, joint angle kinematic relation introduced by momentum conservation, natural constraint in swing motion and preferred values such as β and θ_c are analyzed. Natural Constraints Planner is proposed to organize the internal and external constraints and generate a feasible motion plan with only a preferred β. Compared to the existing methodology, the proposed algorithm are more flexible and generally applicable. The algorithm can adapt configurations with different horizontal and vertical differences and also has the possibility of controlling the energy efficiency, which opens the door of realizing continuous ricochetal brachiation.

ACKNOWLEDGMENT

The research is sponsored by the National Natural Science Foundation of China, Grant No.61503067.

REFERENCES

[1] Swartz.S.M, "Pendular mechanics and the kinematics and energetics of brachiating locomotion," *International Journal of Primatology*, vol. 10, no. 5, pp. 387–418, 1989.

[2] Bertram.JE, Ruina.A, Cannon.CE, Chang.YH, and Coleman.MJ, "A point-mass model of gibbon locomotion," *The Journal of Experimental Biology*, vol. 202, pp. 2609–2617, 1999.

[3] M. W. Gomes and A. L. Ruina, "A five-link 2d brachiating ape model with life-like zero-energy-cost motions," *Journal of Theoretical Biology*, vol. 237, no. 3, pp. 265 – 278, 2005.

[4] J. E. Bertram, "New perspectives on brachiation mechanics," *American Journal of Physical Anthropology*, vol. 125, no. S39, pp. 100–117, 2004.

[5] Y.-H. Chang, J. E. Bertram, and D. V. Lee, "External forces and torques generated by the brachiating white-handed gibbon (hylobates lar)," *American Journal of Physical Anthropology*, vol. 113, no. 2, pp. 201–216, 2000.

[6] F. Michilsens, K. D'Aot, and P. Aerts, "?how pendulum-like are siamangs? energy exchange during brachiation?" *American Journal of Physical Anthropology*, vol. 145, no. 4, p. 581?591, 2011.

[7] V. M. D. Oliveira and W. F. Lages, "Linear predictive control of a brachiation robot," in *2006 Canadian Conference on Electrical and Computer Engineering*, May 2006, pp. 1518–1521.

[8] C. V. Meaclem, S. Gutschmidt, X. Chen, and R. Parker, "Kinematic and dynamic analysis of a brachiating tree-to-tree machine," in *2015 IEEE International Conference on Robotics and Biomimetics (ROBIO)*, Dec 2015, pp. 1311–1316.

[9] T. Fukuda, F. Saito, and F. Arai, "A study on the brachiation type of mobile robot (heuristic creation of driving input and control using cmac)," in *Intelligent Robots and Systems '91. 'Intelligence for Mechanical Systems, Proceedings IROS '91. IEEE/RSJ International Workshop on*, Nov 1991, pp. 478–483 vol.2.

[10] F. Saito, T. Fukuda, and F. Arai, "Swing and locomotion control for a two-link brachiation robot," *Control Systems, IEEE*, vol. 14, no. 1, pp. 5–12, Feb 1994.

[11] F.Saito and T.Fukuda, "A first result of the brachiator iii-a new brachiation robot modeled on a siamang," *MIT Press*, vol. 43, pp. 354–361, 1997.

[12] H.Kajima, Y.Hasegawa, and T.Fukuda, "Learning algorithm for a brachiating robot," *Applied Bionics and Biomechanics*, vol. 1, no. 1, pp. 57–66, 2003.

[13] H. Nishimura and K. Funaki, "Motion control of three-link brachiation robot by using final-state control with error learning," *Mechatronics, IEEE/ASME Transactions on*, vol. 3, no. 2, pp. 120–128, Jun 1998.

[14] A. Meghdari, S. M. H. Lavasani, M. Norouzi, and M. S. R. Mousavi, "Minimum control effort trajectory planning and tracking of the cedra brachiation robot," *Robotica*, vol. 31, no. 7, pp. 1119–1129, 10 2013.

[15] J. Nakanishi and T. Fukuda, "A leaping maneuver for a brachiating robot," in *Robotics and Automation, 2000. Proceedings. ICRA '00. IEEE International Conference on*, vol. 3, 2000, pp. 2822–2827 vol.3.

[16] J. Zhao, T. Zhao, N. Xi, M. W. Mutka, and L. Xiao, "Msu tailbot: Controlling aerial maneuver of a miniature-tailed jumping robot," *IEEE/ASME Transactions on Mechatronics*, vol. 20, no. 6, pp. 2903–2914, Dec 2015.

[17] H. Sone and D. Nenchev, "Reactionless camera inspection with a free-flying space robot under reaction null-space motion control," *Acta Astronautica*, vol. 128, pp. 707 – 721, 2016.

[18] W. Xu, J. Peng, B. Liang, and Z. Mu, "Hybrid modeling and analysis method for dynamic coupling of space robots," *IEEE Transactions on Aerospace and Electronic Systems*, vol. 52, no. 1, pp. 85–98, February 2016.

[19] H. L. Richard W. Timm, "Periodicity emerges from evolved energy-efficient and long-range brachiation," *Mechanical and Aerospace Engineering,Cornell University, Ithaca, NY*, 2004.

[20] C. Hongtai, Z. Yini, and Z. Xiaohua, "Dynamical servo control and symmetrical virtual constraints method for the acrobot," *Acta Automatica Sinica*, vol. 36, no. 11, pp. 1594–1600, 2010.

Authorized licensed use limited to: University of Pennsylvania. Downloaded on May 23,2025 at 14:26:01 UTC from IEEE Xplore. Restrictions apply.